Catalysis Science & Technology

Accepted Manuscript

ROYAL SOCIETY OF CHEMISTRY

www.rsc.org/catalysis

Journal Name

RSCPublishing

ARTICLE

Selective Catalytic Reduction of NO with NH_3 over Novel Iron–Tungsten Mixed Oxide Catalyst in a Broad Temperature Range

Xiang Li, Junhua Li*, Yue Peng, Tao Zhang, Shuai Liu and Jiming Hao

Cite this: DOI: 10.1039/xoxxoooooox

Received ooth January 2012,
Accepted ooth January 2012

DOI: 10.1039/xoxxoooooox

www.rsc.org/

A series of novel FeW(x) catalysts with different Fe/W molar ratios prepared by the co-precipitation method were investigated on selective catalytic reduction (SCR) of NO_x with NH_3. Among the tested catalysts, the FeW(5) shows the highest catalytic activity, nearly 100% of NO conversion and N_2 selectivity from 250 to 450 °C, and good H_2O/SO_2 durability above 300 °C. After the introduction of WOx species, the lattice structure change of hematite phase and high dispersion of WOx on the surface of catalysts are observed for FeW(x) catalysts. The abundance of surface adsorbed oxygen arises from charge imbalance and unsaturated chemical bonds formation by the interaction between iron oxide species and tungsten oxide species. The Brønsted acid sites are mainly supplied by the W-OH bond, while the Lewis acid sites are related to iron oxide species. Meanwhile the addition of WO_x not only leads to the formation of lower-valent iron species and consequently decreases the Lewis acidity, thereby improving N_2 selectivity, but also enhances the stability of surface acid sites and adsorption of monodentate nitrite and NO_2 species, which account for the excellent catalytic performance of FeW(5) at low temperature. According to the reaction details, Brønsted acid sites play a leading role at low temperature and Lewis acid sites may be the major active centers at high temperature in the SCR process for FeW(x) catalysts.

1. Introduction

Nitrogen oxides (NO_x) from exhaust gases of stationary (coal-fired power plants) and mobile sources (lean-burn diesel engines) have become major sources of air pollution which can result in a series of severe environmental problems, such as photochemical smog, acid rain and ozone depletion, and threaten human mainly because of strong respiratory toxicity.[1-3] Selective catalytic reduction of NO_x with NH_3 (NH_3-SCR) is named as an effective and economical method and has become the most widely used deNO_x technology.[4] However, the commercial vanadia-based catalysts (V_2O_5/TiO_2, V_2O_5–WO_3/TiO_2 or V_2O_5–MoO_3/TiO_2) have many disadvantages: high cost, narrow temperature window (350-400 °C), the toxicity of V_2O_5 to the environment and low N_2 selectivity at high temperature.[5,6]

Many researchers have focused on developing new SCR catalysts to substitute the conventional vanadia-based catalysts. Among them, iron-based catalysts, such as Fe-Ti,[7,8] Fe-Zr,[9] Fe-Mn,[10] Fe-V,[11] Fe-Ce,[12] Fe–Ti–V,[13] Fe(S)-Ti[14] and Fe-zeolites,[15] have caught more attentions for their high NH_3-SCR activity at low temperature, non-toxicity relative to vanadium oxide and good SO_2 durability. It is noteworthy that pure iron oxide catalyst exhibits good NH_3-SCR activity because of its excellent reducibility and mobility of surface active oxygen, but is subject to relatively low surface acidity, poor resistance to H_2O and SO_2 and low selectivity to N_2 above 350 °C.[16] Additionally, a large number of active ingredients, such as Mn, Ce and V, introduced not only make iron oxide fail to display fullest catalytic potential but also raise the cost of catalysts. Therefore, introducing the moderate and appropriate auxiliaries into pure Fe_2O_3 catalyst system can be a better choice for improving the above situation.

Many promoting effects of the W component for the SCR catalysts have been observed recently. The advantages of WOx to vanadia-based can be summarized as follows: (1) increasing surface acidity drastically and partly delaying the loss of BET surface area;[17,18] (2) preventing excessive VO_x island formation and the transformation from monomeric vanadyl to crystalline V_2O_5 during aging;[19] (3) creating a mixed surface phase with small surface vanadium and tungsten oxide entities.[20] Recently, some transition metal-tungsten mixed oxide catalysts exhibit relatively high activity for NO_x conversion. Liu et al. reported that, for MnWOx catalysts, W addition decreased the particle size of MnOx phase, increased the surface acidity and facilitated the NO/NH_3 oxidation.[21] Shan et al. exploited novel Ce-W mixed oxide catalysts, and found a synergistic effect between Ce and W species was the main reason for excellent NH_3-SCR activity.[22]

However, poor SO_2 durability of MnOx and expensive cost of rare earth CeO_2 limit their application for NH_3-SCR, and thus iron-based catalysts may be a better candidate one to substitute the conventional vanadia-based catalyst. In this paper, tungsten doped iron-based catalysts were synthesized by co-precipitation method. The activities for the SCR of NO_x with NH_3 and H_2O/SO_2 durability at the relatively high space velocity of 60000 h^{-1} were investigated. The FeW(x) catalyst exhibited an outstanding catalytic performance at the temperature range 250-450 °C. The effects of WO_x on the structural and chemical properties of the catalysts were studied using N_2 physisorption, X-ray diffraction (XRD), Raman spectra, X-ray photo electron spectroscopy (XPS), H_2 temperature-programmed reduction (H_2-TPR), NH_3 temperature-programmed desorption (NH_3-TPD) and ammonia adsorption infrared spectroscopy. Finally, the reactivity of surface-adsorbed NH_3 and NO_x species on the catalyst was investigated using in situ diffuse reflectance infrared Fourier transform spectroscopy (in situ DRIFTS)..

2. Experimental

2.1 Catalyst Preparation

The co-precipitation method was applied to the preparation of FeO_x-WO_x using $Fe(NO_3)_3{\cdot}9H_2O$ and $(NH_4)_6W_7O_{24}{\cdot}6H_2O$ as precursors and $NH_3{\cdot}H_2O$ as the precipitant. Typically, $NH_3{\cdot}H_2O$ solution (25 %) was dropped into the stoichiometric solution of $Fe(NO_3)_3{\cdot}9H_2O$ and $(NH_4)_6W_7O_{24}{\cdot}6H_2O$ with continuous stirring until pH value of the solution was 7. After washed with deionized water for several times, the precipitates were collected and then dried at 80 °C overnight for the removal of water. The final samples were calcined at 500 °C for 3 h in air with a heating rate of 2 °C·min^{-1}. The catalysts can be denoted as FeW(x), where x means the molar ratio of Fe/W. Meanwhile, pure Fe_2O_3 and WO_3 were also prepared as a comparison using the same preparation method.

2.2 Catalytic Performance

The activity test of FeW(x) catalysts were completed in the fixed-bed reactor with a quartz tube (6 mm internal diameter). The reaction condition was as follow: 0.2 g catalyst (40-60 mesh), 500 ppm NH_3, 500 ppm NO, 3% O_2, total gas flow rate of 200 ml·min^{-1} balanced by N_2. The corresponding gas hourly space velocity (GHSV) was 60000 h^{-1}, and the range of temperature was from 150 °C to 450 °C. According to the concentrations of inlet and outlet NO_x (x=1, 2), NH_3 and N_2O, the NO conversion, N_2 selectivity and the pseudo-first order rate constant (k) were calculated by the formula as follow:

$$\boldsymbol{X_{NOx}} = \frac{\boldsymbol{C_{NOx(in)} - C_{NOx(out)}}}{\boldsymbol{C_{NOx(in)}}} \times \mathbf{100}\ \% \quad (1)$$

$$\boldsymbol{S_{N_2}} = \left[\mathbf{1} - \frac{\boldsymbol{2C_{N_2O(out)}}}{\boldsymbol{C_{NO_X(in)} + C_{NH_3(in)} - C_{NO_X(out)} - C_{NH_3(out)}}}\right] \times \mathbf{100}\ \% \quad (2)$$

$$\boldsymbol{k} = -\frac{\boldsymbol{F}}{\boldsymbol{V}}\mathbf{ln}(\mathbf{1} - \boldsymbol{X}) \quad (3)$$

Where $C_{NO(in)}/C_{NH3(in)}$ and $C_{NO(out)}/C_{NH3(out)}$ were the concentrations of gaseous NO/NH_3 in the inlet and outlet, respectively; $C_{N2O(out)}$ was the concentration of gaseous N_2O in the outlet; F is the total flow rate (cm^3 s^{-1}), V is the volume of the catalyst (cm^3) and X is the relative NO conversion.

2.3 Catalytic Characterization

The XRD measurement (Rigaku, D/max-2200/PC) between 10° and 80° at a step rate 5 °C/min reflected the crystal structure using Cu Kα radiation, where interplanar spacing was calculated. Raman spectra were measured using a Raman microscope (InVia Reflex, Renishaw) under the 532 nm excitation laser light. N_2 adsorption–desorption experiments were performed measured using a Quantachrome Nova automated gas sorption system under liquid N_2 environment (77K). The results of XPS measurement were obtained on an ESCA system from VG Scientific with 300 W Al Kα radiations. The H_2-TPR (temperature-programmed reduction) test was carried out using Micromeriitics ChemiSorb 2720 TPx with 0.05 g catalyst in a H_2/Ar flow at 10 °C·min^{-1} up to 1000 °C following the pretreatment with He at 350 °C for 1 h. The NH_3-TPD (temperature-programmed desorption) test was recorded using a FTIR spectrometer (MKS, MultiGas 2030HS) with 0.05 g catalyst. There were four steps in this test: (1) pretreatment using N_2 at 350 °C for 1 h, (2) cooling down to 100 °C followed by the saturation adsorption of NH_3; (3) removing NH_3 of physisorption by N_2 purging; (4) starting the desorption of NH_3 under N_2 environment at a rate of 10 °C·min^{-1}up to 700 °C. In-situ DRIFTS spectra were performed on FTIR, Nicolet NEXUS 870. Before test, the catalyst was preheated at 350 °C for 1 h in N_2 at a flow of 100 mL·min^{-1} to remove adsorbed impurities, and DRIFTS spectrum were collected by accumulating 32 scans with a resolution of 4 cm^{-1}.

3. Results and discussion,

3.1 Reaction performance

The NO_x conversions and N_2 selectivity of the FeW(x) catalysts with different molar ratios of Fe to W are shown in Fig. 1 (a) and (b). Experimental results show that the highest NO_x conversion is only 65% when pure Fe_2O_3 is used as SCR catalyst at 150-450 °C, and that the addition of W can significantly increase NO_x conversion in the whole temperature range, although which of the pristine WO_3 is just above 40%. It is found that the NO_x conversion and N_2 selectivity are greatly improved to nearly 100% when the Fe/W molar ratio reaches up to five at 250-400 °C. With increase of Fe content, the operation temperature window decreases slightly for the FeW(10) catalyst, but FeW(10) catalyst keeps high N_2 selectivity as before (as shown in Fig. 1b). In order to compare the low-temperature catalytic performance, the Arrhenius plot for SCR performance (Fig. 1c), reaction rate constants (k) and

the apparent activation energies (Ea) (Table 1) of the FeW(x) catalysts (x=1, 3, 5 and 10) are also researched. As shown in Fig.1c and Table 1, The FeW(5) exhibits a higher reaction rate

Table 1. Physical and kinetic property of FeW(x) catalysts.

Catalyst	S_{BET} (m^2/g)	Vp (cc/g)	Dp (nm)	k[a] (s^{-1})	Ea (kJ/mol)
FeW(1)	9. 8	0.014	4.9	2.01	42.4
FeW(3)	31.2	0.083	8.6	5.95	64.4
FeW(5)	49.2	0.119	7.7	12.37	38.5
FeW(10)	42.3	0.106	8.0	6.7	54.7

[a] Reaction rate constants (k) of FeW(x) catalysts were calculated at 200 °C..

($k = 12.37\ s^{-1}$) and lower value of the slope of the fitting line than those of other three catalysts, meaning that it has the highest low-temperature SCR catalytic activity and the smallest energy barriers (Ea = 38.5 kJ/mol) among the four kinds of catalysts. This suggests that a synergistic effect may exist between Fe and W species for the NH_3-SCR reaction.

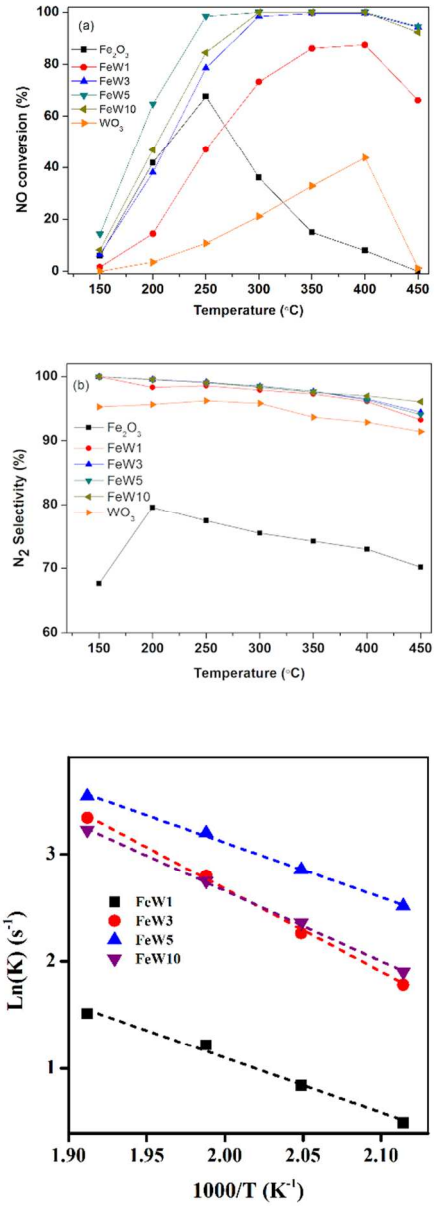

Figure 1. (a) NO conversion using FeW(x)、Fe_2O_3 and WO_3 catalysts; (b) N_2 selectivity in the SCR reaction; (c) The Arrhenius plot for SCR performance over the FeW(x) catalysts (x=1, 3, 5 and 10). Reaction condition: [NO] = [NH_3] = 500 ppm, [O_2] = 3%, total flow rat e= 200 mL/min, GHSV = 60000 h^{-1}.

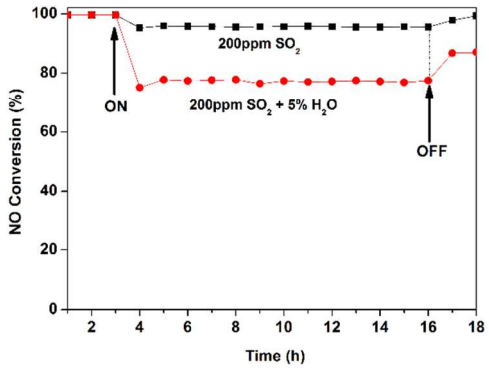

Figure 2. The influence of SO_2 and SO_2/H_2O on NO conversion in the SCR reation over FeW(5) catalyst at 300 °C. Reaction condition: [NO] = [NH_3] = 500 ppm, [SO_2] = 200 ppm, [O_2] = 3%, [H_2O] = 5%, total flow rate = 200 mL/min, GHSV = 60000 h^{-1}.

The FeW(5) catalyst is chosen to investigate the SO_2 and H_2O durability, because SO_2 and H_2O in the exhaust usually lower the NH_3-SCR catalytic activity. The influences of 200 ppm SO_2 and 5 vol% H_2O on the catalytic performance of the FeW(5) catalyst are studied at 300 °C for 18h and the corresponding results are illustrated in Fig. 2. When 200 ppm SO_2 is introduced, the NO_x conversion of FeW(5) catalyst shows a slight decrease, then becomes stable (at about 95%), and after removing SO_2 the conversion recovers to nearly 100% as initial. However, when 5 vol% H_2O is introduced with 200 ppm SO_2 simultaneously, NO_x conversion decreases obviously and still maintains at approximately 78 %. This decrease is related with the formation of $(NH_4)_2SO_3$ or NH_4HSO_4, which deposits on the surface of the catalyst and then blocks the partial active sites.[23] The above results suggest that the FeW(5) catalyst has a certain SO_2 and H_2O durability above 300 °C.

3.2 Structure characterization

The N_2 adsorption–desorption isotherms of the FeW(x) catalysts are shown in Fig. 3, and data of surface area, pore volume and pore diameter are also listed in Table 1. As seen in Fig. 3, all the FeW(x) catalysts except FeW(1) show typical IV curves and H1 type hysteresis loop, indicating the formation of the cylindrical mesoporous structure and narrow pore distribution. With increased Fe content, the average pore diameter increases correspondingly, but the surface area improves from initial 9.8 to 49.2 m^2/g (FeW(5)) firstly, and then downs to 42.3 m^2/g (FeW(10)), whose trend is consistent with the pore volume and NO_x conversion at the low temperature range (150-250°C). So it implies that the low-temperature SCR activity is related to the apparent surface properties to some extent. Noting that the values of the surface areas for all four samples are lower than 50 m^2/g, which is due to the structure sintering or collapse. Therefore, relatively low BET parameters exhibit that it should not be the key factor to determine the activity.

To obtain structural information of the FeW(x) catalysts, XRD patterns and Raman spectra are studied and shown in Fig. 4. There are some peaks appearing at 24.1°, 33.1°, 35.6°, 40.9°, 49.4°, 54.1°, 57.5° 62.5° and 64.0°, which belong to hematite Fe_2O_3 (α-Fe_2O_3, PDF33-0664) illustrated in Fig.4a. With increased WO_3 content, the diffraction peaks are broaden and weak, indicating that the average grain sizes of Fe_2O_3 on these catalysts decrease; meanwhile, the main (2θ = 33.1°) peak of FeW(10) shifts toward higher angle direction, and some small characteristic peaks attributed to Fe_2WO_6 (2θ = 26.9°, 30.7° and 36.7°) and ɤ-Fe_2O_3 (2θ = 63.3°) appear; no visible phase of WO_3 species can be observed. These results signify: (1) the WO_3 species are highly dispersed on the surface of α-Fe_2O_3, but it is noted that a higher crystallizing degree (hematite) shows for FeW(10) than other samples, which may be adverse to NH_3-SCR activity; (2) some of the tungsten atoms may penetrate into the lattice structure of hematite phase (surface or subsurface) and form Fe-O-W bond because of strong interaction. Additionally, because the ionic radius of Fe^{3+} (0.55 Å) is a little smaller W^{6+} (0.60 Å) and they are both six-coordinated with octahedron geometry, the replacement of Fe^{3+} by W^{6+} to form a solid solution can be expected. Furthermore, when the Fe/W molar ratio drops to 1, sharp peaks disappear and a broad peak (2θ = 18.8-38.8°) arises. The angle deflection of the diffraction peak disappears. This suggests a transformation from the bulk, regular crystals to an amorphous structure on the catalyst surface and the interaction between iron oxide species and tungsten oxide species weaken.

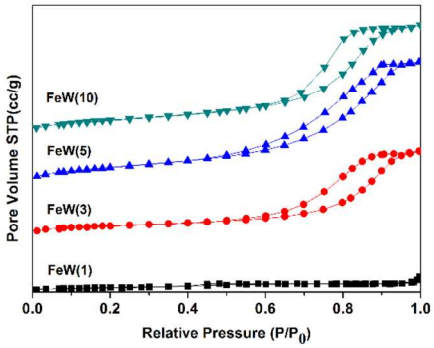

Figure 3. Nitrogen adsorption-desorption isotherms of the FeW(x) catalysts.

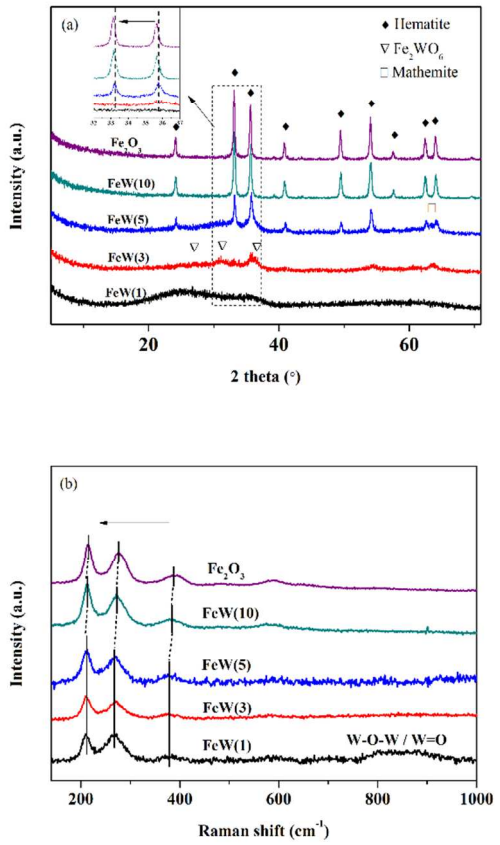

Figure 4. (a) XRD patterns and (b) Raman spectra of the FeW(x) catalysts.

Raman spectroscopy is the method that has provided most information on the speciation of the surface iron and tungsten species. Two sharp and a broad peaks of FeW(10) spectrum are displayed in Fig.4b at approximately 213 (A_{1g} mode), 273 and 380 cm^{-1} (E_g modes) is associated with α-Fe_2O_3 hematite.[24] Obviously, these peaks shift towards lower wavenumber (smaller bond energy) direction when Fe/W ratio reduce to 5. This tendency is in accordance with the XRD pattern results, indicating the increase of the Fe-O bond length by the introduction of WOx and formation of Fe-O-W bond. However, with increased Fe content, peak positions associated with α-Fe_2O_3 are no longer move. A possible explanation is that the concentration of WO_x in the solid solution reaches a stable value and that excess WOx will not incorporate into the matrices of hematite phase to form more Fe-O-W bond. Subsequently, two weak peaks due to the WO_x species can be observed for FeW(1) catalyst. The broad peak centered at approximately 804 cm^{-1} is due to the microcrystalline WO_3,[25] and the weaker one at approximately 884 cm^{-1} can be attributed to the vibration of W−O,[26] meaning a large amount of tungsten oxide species exist in isolation on the FeW(1) catalyst. Thus, combining with the XRD, Raman and SCR activity, the strong interaction between FeOx and WOx species and high dispersion of WOx in the mixed oxide catalyst play an important role in the NH_3-SCR reaction.

3.3 Redox properties

H_2-TPR is a widely used technique to investigate the redox properties of the catalysts. Fig. 5 shows the H_2-TPR profiles of the four FeW(x) catalysts in the temperature range of 150–1000 °C. In view of the weaker reducibility and less quantity of WOx species, the two peaks across 550–670 °C and 700–950 °C can correspond to the following reduction steps: Fe_2O_3-Fe_3O_4 and Fe_3O_4-FeO, respectively.[26,27] The onset consumption order is FeW(5) (555 °C) < FeW(10) (574 °C) < FeW(3) (579 °C) < FeW(1) (668 °C), representing that H_2 reduction is promoted first, and then suppressed with decreased concentration of WO_3. And BET surface area may be an important factor to determine the onset H_2 consumption, because the reduction of catalyst is initiated from the surface. However, The H_2 consumption amounts (the total peak areas) are significantly decreased by the tungsten doping. A reasonable explanation is that iron oxide species having stronger reducibility are replaced by more stable tungsten oxide ones.

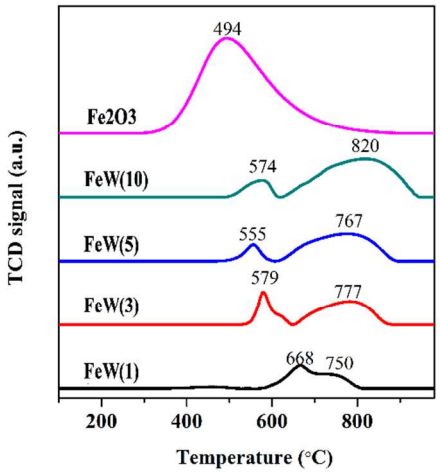

Figure 5. H_2-TPR profiles of the FeW(x) catalysts.

To further characterize chemical environment of O and Fe on the surface of the FeW(x) catalysts, the XPS spectra of O1s and Fe 2p3/2 for the four catalysts are investigated and the results are exhibited in Fig. 6 and Table 2. According to the Fig. 6a, the sub-bands at lower binding energy (529.7–530.2 eV) correspond to the lattice oxygen (O^{2-},denoted as O_β), and the ones at higher binding energy (531.5–532.2 eV) are attributed to the surface adsorbed oxygen denoted as Oα, such as O^- and O^{2-}.[28] The latter is often thought to be more reactive in oxidation reactions because of its higher mobility, and researcher have suggested that a high $O_\alpha/(O_\alpha + O_\beta)$ ratio is beneficial for the NO oxidation to NO_2 in the SCR reaction at low temperatures and thereafter facilitates the "fast SCR" reaction.[29] As is presented in Fig.5b, it is clear that FeW(5) catalyst has the greatest amount of chemisorbed oxygen species ($O_\alpha/(O_\alpha + O_\beta)$=29.4%) among the FeW(x) catalysts. Consequently, its best activity for the oxidation of NO to NO_2

than others can be a reasonable explanation for having outstanding NH_3-SCR catalytic activity at low temperatures.

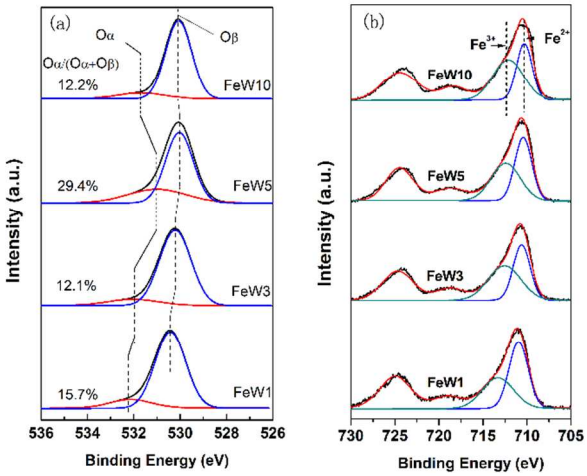

Figure 6. O1s (a) and Fe2p 2/3 (b) from XPS spectra of the FeW(x) catalysts.

The $Fe2p_{3/2}$ peak could be separated into two peaks by the same peak fitting deconvolution technique (Fig.6b), and the relative surface contents of Fe^{2+}, Fe^{3+} and Fe_{total} for each sample are also calculated and summarized in Table 2. The peaks centered at ~713 eV can be assigned to Fe^{3+} and the ones at~711eV to Fe^{2+}.[30] As listed in Table 2, with increased W doping, the surface Fe^{2+} content is gradually increased, reaches the maximum 11.35% (FeW(5)), then reduces to 7.93% (FeW(1)). Many researchers considered that the emergence of new specie with intermediate valence was a major reason for the enhancement of reaction activity. Zhan et al. found that the better low-temperature reducibility properties of the MnO_2 doped Fe_2O_3 hollow nanofiber were mainly related to the concentrations of Fe^{2+} and Mn^{3+} cations, which can lead to the increase in oxide defects or hydroxyl-like groups.[31] Peng et al. had confirmed that the Ce^{3+} cations were slightly increased by the WO_3 loading and the W-O-Ce bond was formed due to the strong interactions between the tungsten species and the surface ceria for CeO_2-WO_3 system.[32] Hence the presence and quantity of Fe^{2+} should be important to create charge imbalance, vacancies, interactions and unsaturated chemical bonds on the catalyst surface, which will lead to the increase the relative content of surface chemisorbed oxygen. The introduction of tungsten oxide species has an obvious positive effect for pure Fe_2O_3, altering the chemical environments and redox properties and thus enhancing the SCR performances.

3.4 Surface acidities

It is proposed that the catalyst surface acidity is a key factor in the SCR reaction which can be measured by DRIFTS spectra of NH_3 adsorption and NH_3-TPD characterization methods. Fig. 6a shows the DRIFT spectra of NH_3 adsorption on the FeW(x) catalysts at 200 °C. Several bands at 1213, 1426, 1603, 1672, 3164, 3256 and 3352 cm^{-1} and some negative bands in the range of 3605-3655 cm^{-1} are detected. The bands at 1603 and 1213 cm^{-1} can be attributed to asymmetric and symmetric bending vibrations of the N-H bonds in NH_3 coordinately linked to Lewis acid sites; and the bands at 1426 and 1672 cm^{-1} are assigned to coordinated NH_4^+ chemisorbed on Brønsted acid sites.[33] In the N-H stretching region,[34] bands are observed at 3352, 3256, and 3164 cm^{-1}. The negative bands centered at approximately 3647 cm^{-1} are also found, which can be ascribed to surface O-H stretching.[7] Brønsted and Lewis acidities of FeW(x) catalysts at 200 °C are obtained by calculating the integrated peak areas of 1426 and 1213 cm^{-1} in the DRIFTS spectra and the results are listed in Table 3. It is noteworthy that the introduction of WO_x species into α-Fe_2O_3 leads to the increase of Brønsted acid sites, while FeW(5) sample has the largest number of Brønsted acid sites (8.4 a.u.) than the other ones. These results are similar to the conclusions of J. Engweiler's research on V_2O_5-WO_3/TiO_2 catalysts, who held that surplus tungsten content was converted into crystalline WO_3, which is negative to the formation of acid sites.[26] Combined with the XRD and Raman results, the W-OH bond origin from the introduction of WOx specie is related to the Brønsted acid sites, and redundant WOx addition is adverse to the formation of acid sites and cover the existing acid sites. Additionally, Lewis acid sites of catalysts lessen significantly in parallel with the amount of Fe_2O_3 reduced, which hints that Lewis acid sites are mainly supplied by iron oxide species.

To further investigate the acid strength, the NH_3 desorption from Lewis and Brønsted acid sites are performed on FeW(5) in the temperature range of 50 to 350 °C (Fig. 6b). Both peak intensities due to Lewis and Brønsted acid sites decrease with increased temperature, and the Lewis acid sites exhibit higher stability. compared with the Brønsted acid sites: the band at 1421 cm^{-1} nearly disappears, whereas the band at 1227 cm^{-1} can be still observed at 350 °C in N_2. Therefore, the high stability of Lewis acidic sites on FeW(x) catalysts is a possible reason for the excellent catalytic activity at high temperatures.

Table 2. XPS results of FeW(x) catalysts.

Catalyst	Surface atomic concentration (%)						
	Fe^{2+}	Fe^{3+}	Fe_{total}	W	$O_α$	$O_β$	O_{total}
FeW(1)	7.93	7.27	15.2	11.35	11.53	61.92	73.45
FeW(3)	9.75	11.73	21.48	6.43	8.72	63.37	72.09
FeW(5)	11.35	11.48	22.83	5.14	21.18	50.85	72.03
FeW(10)	9.96	13.98	23.94	4.34	8.75	62.97	71.72

Table 3. NH_3 desorption amount and Lewis and Brønsted acidities at 200 °C of FeW(x) catalysts.

Catalyst	The amount of NH_3 desorption μmol/g				The amount of acid sites a.u. (200 °C)	
	weak acid sites	Medium acid sites	Strong acid sites	Total	Lewis aciditie s	Brønsted acidities
FeW(1)	3.4	8.9	9.8	22.1	1.3	2.3
FeW(3)	4.6	9.2	10.0	23.8	3.7	4.3
FeW(5)	8.0	13.4	14.8	36.2	5.3	8.4
FeW(10)	7.7	15.2	19.5	42.4	9.6	8.1

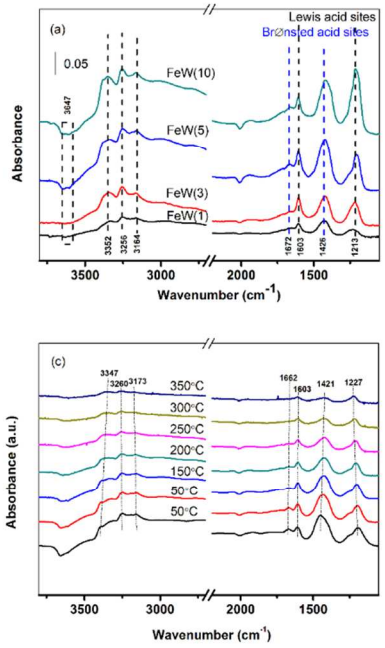

Figure 6. DRIFT spectra of (a) NH3 adsorption at 200 °C of the FeW(x) catalysts and (b) the NH3 desorption of FeW(5) catalyst at the temperature range of 50-350 °C.

The effect of the amount and strength of the acid sites on the activity of the FeW(x) catalysts in NH_3–TPD experiments is illustrated in Fig. 7. As can be seen from the curves, all the catalysts display three NH_3 desorption peaks, which is accordance with Zhang's research on the Fe_2O_3 and Fe-V-O_x catalysts.[11] The first peak at around 239-256 °C can be attributed to weak acid sites (weakly bonded NH_3); similarly, the other two large ammonia desorption peaks located at 314-325 and 429-451 °C can be assigned to medium and strong acid sites, respectively. Meanwhile, the amounts of different kinds of acid sites on FeW(x) catalysts obtained by calculating the integrated peak are correspondingly listed in Table 3. With increased Fe content, the amounts of medium and strong acid sites and the total acidity of the FeW(x) catalysts are increased markedly, while the order for the amount of weak acid sites is in the sequence: FeW(5) (8.0 μmol/g) > FeW(10) (7.7 μmol/g) > FeW(3) (4.6 μmol/g) > FeW(1) (3.4 μmol/g), keeping goodconsistence with the results of the NO_x conversions at 150-250 °C as noted above. In addition, combined with the IR results in Fig. 6b, the weak acid sites should be assigned to ammonia adsorbed on both Lewis and Brønsted acid sites (main components), because the ammonia peak on both the Lewis and Brønsted acid sites has almost remained between 50 and 250 °C. In the higher temperature range, the intensity of the ammonia adsorption peak on Brønsted acid sites disappear drastically, and Lewis acidic sites gradually become the major ingredient for ammonia adsorbed. Similarly, the strong acid sites are provided by ammonia adsorbed on the Lewis acid sites and the medium acid sites are composed of both Brønsted and Lewis acid sites simultaneously. Since Brønsted acidities were obviously larger than Lewis acidities at 200°C (Table 3), Brønsted acid sites may play a leading role at low temperature and Lewis acid sites may be the major active centers at high temperature for FeW(x) catalysts.、

3.5 Reaction details at low temperature

The mechanism of the SCR reaction over FeW(5) catalysts are studied using in situ DRIFTS at 200 °C (shown in Fig. 8). As illustrated in Fig. 8a, the catalysts are first treated with NH_3/N_2 for 1 h, followed by purging with N_2 for 30 min. The peaks attributed to coordinated NH_3 bound to Lewis (1213 and 1602 cm^{-1}) and ionic NH_4^+ bound to Brønsted (1426 and 1672 cm^{-1}) acid sites can be observed. After NO + O_2 passed over the catalyst, Lewis acidity is lost rapidly, and Brønsted acidity diminishes within 5 min, which implies that both Lewis and Brønsted acidities are reactive at 200 °C. Simultaneously, the peak at 1603 cm^{-1} is significantly increased, while other peaks at 1545, 1356 and 1273 cm^{-1} as well as a negative peak centered at 1240 cm^{-1} are obtained after 5 min. The peak at 1603 cm^{-1} can be assigned to adsorbed NO_2; the peaks at 1545 and 1356 cm^{-1} should be attributed to monodentate nitrite; and the negative bands at 1240 cm^{-1} are associated with residual bridging nitrate species in synthesized FeW(x) catalysts with $Fe(NO_3)_3$ as precursor.[35] When the reactants are introduced to the FeW(5) catalyst in the reversed order, the band (1603, 1547, 1366 and 1267 cm^{-1}) attributed to the nitrite and adsorbed NO_2 species can be observed on the catalyst after purging NO and O_2. When NH_3 is introduced for 1 min, the monodentate nitrite species decrease obviously and totally disappear after 3 min. At the same time, the band due to adsorbed NO_2 begins to be replaced by the larger band at 1603 cm^{-1} assigned to Lewis acid sites. After the catalyst is purged with NH3 for 5 min, the catalyst surface is mainly covered by ammonia species. On the basis of the above results, it can be concluded that the NH_3 species bonded to the Brønsted and Lewis acid sites can

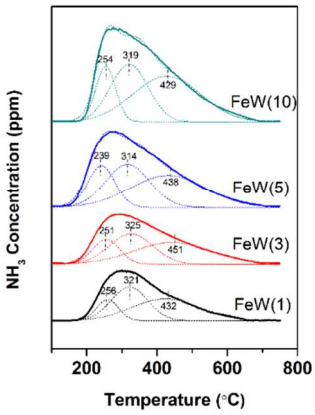

Figure 7. NH_3-TPD curves of the FeW(x) catalysts.

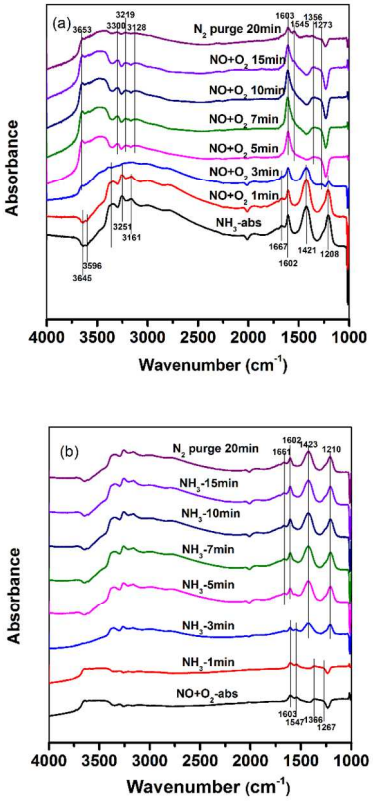

Figure 8. In situ DRIFT spectra of FeW(5) catalyst at 200 °C under different atmospheres: (a) the dehydrated catalyst was first treated by NH_3, then NO + O_2 was added; (b) a reversed order of the gasses indicated was applied.

react with monodentate nitrite and adsorbed NO_2 species in the SCR reaction at 200 °C, which should be considered the SCR reaction through the Langmuir–Hinshelwood mechanism.[36] It can be approximately described as follows:

$$NH_3(g) \leftrightarrows NH_3(ad) \quad (4)$$

$$NO(g) \leftrightarrows NO\ (ad) \quad (5)$$

$$NO + 1/2\ O_2 \leftrightarrows NO_2(ad) \quad (6)$$

$$\equiv Fe^{3+} + O^{2-} + NO(ad) \rightarrow \equiv Fe^{2+} + NO_2^- \quad (7)$$

$$NO_2(ad) / NO_2^- + NH_3(g) \rightarrow N_2 + H_2O \quad (8)$$

$$\equiv Fe^{2+} + 1/4\ O_2 \rightarrow \equiv Fe^{3+} + 1/2\ \equiv O^{2-} \quad (9)$$

Reaction (4) is the adsorption of gaseous ammonia on the Brønsted acid sites or Lewis acid sites to form adsorbed ammonia species ionic NH_4^+ and coordinated NH_3, respectively. It is generally acknowledged that the SCR reaction starts with the adsorption of NH_3 because it is stronger than the adsorption of NO + O_2.[10] Reaction (5) and (6) stand for the adsorption of gaseous NO and NO_2. Then the adsorbed NO is oxidized by Fe^{3+} cations on the surface to form adsorbed monodentate nitrite NO_2^- and Fe^{2+} cations form (reactions (7)). After that, the adsorption of NO_2 and the formed NO_2^- on catalyst is reduced by adsorbed ammonia species to form N_2 and H_2O (reaction (8)). At last, reactions (9) are the re-oxidization of transformed Fe^{2+} species, and the introduction of WO_x may speed up the reaction (4), (6), (7) and (9) owing to the promotion of amounts of acid sites and surface adsorbed oxygen.

Conclusions

In this paper, novel FeW(x) catalysts with different WO_x doping content were prepared by the co-precipitation method, which shows highly active for the selective catalytic reduction of NO with NH_3. The FeW(5) catalysts show the highest activity, excellent N_2 selectivity and good H_2O/SO_2 durability at 250-450 °C with a space velocity of 60000 h^{-1}. Meanwhile, tungsten atoms can penetrate into the lattice structure of hematite phase and some interaction is found between iron oxides and tungsten oxides. While redundant WOx addition is adverse to the reaction activity and cover the acid sites because large amount of tungsten oxide species exist in isolation. The FeW(5) have the largest BET surface area and number of surface adsorbed oxygen, Brønsted acidity and weak acid sites that contributed to facilitate the SCR reaction. The abundance of surface adsorbed oxygen arise from the formations of charge imbalance, vacancies and unsaturated chemical bonds on the catalyst surface by the interaction between iron oxide species and tungsten oxide species. The Brønsted acid sites and Lewis acid sites are related to are provided by the W-OH bond and iron oxide species, respectively. On the basis of the DRIFTS analysis, the NH_3 species bonded to the Brønsted and Lewis acid sites can react with monodentate nitrite and adsorbed NO_2 species in the SCR reaction following Langmuir–Hinshelwood mechanism at 200 °C, and Lewis acid sites can be the major active centers in the SCR process at high temperature. Therefore, FeW(x) could be a promising catalyst to substitute the conventional vanadium based catalyst for the control of NOx emission.

Acknowledgements

This work was financially supported by National Natural Science Foundation of China (21325731 & 51478241), National High-Tech Research and Development (863) Program of China (2013AA065401 & 2013AA065304), and China Postdoctoral Science Foundation (2013M530643).

Notes and references

State Key Joint Laboratory of Environment Simulation and Pollution Control, School of Environment, Tsinghua University, Beijing, 100084, China
Tel.: +86 10 62771093, Fax: +86 10 62771093
E-mail: lijunhua@tsinghua.edu.cn.

1. H. Bosch and F. Janssen, *Catal. Today*, 1988, **2**, 369-379.
2. B. Jiang, Y. Liu and Z. Wu, *J. Hazard. Mater.*, 2009, **162**, 1249-1254.
3. K. Mathisen, D. G. Nicholson, A. N. Fitch and M. Stockenhuber, *J. Mater. Chem.*, 2005, **15**, 204-217.
4. J. E. Parks, *Science*, 2010, **327**, 1584-1585.
5. G. Busca, L. Lietti, G. Ramis and F. Berti, *Appl. Catal. B- Environ*, 1998, **18**, 1-36.
6. G. Qi, R. T. Yang and R. Chang, *Appl. Catal. B- Environ*, 2004, **51**, 93-106.
7. F. Liu, H. He, Y. Ding and C. Zhang, *Appl. Catal. B- Environ*, 2009, **93**, 194-204.
8. S. Yang, J. Li, C. Wang, J. Chen, L. Ma, H. Chang, L. Chen, Y. Peng and N. Yan, *Appl. Catal. B- Environ*, 2012, **117**, 73-80.
9. N. Apostolescu, B. Geiger, K. Hizbullah, M. Jan, S. Kureti, D. Reichert, F. Schott and W. Weisweiler, *Appl. Catal. B- Environ*, 2006, **62**, 104-114.
10. S. Yang, C. Wang, J. Li, N. Yan, L. Ma and H. Chang, *Appl. Catal. B- Environ*, 2011, **110**, 71-80.
11. P. Zhang and D. Y. Li, *Catal. Lett.*, 2014, **144**, 959-963.
12. X. Zhibo, L. Chunmei, G. Dongxu, Z. Xinli and H. Kuihua, *J. Chem. Technol. Biotechnol.*, 2013, **88**, 1258-1265.
13. S. Yang, C. Wang, J. Chen, Y. Peng, L. Ma, H. Chang, L. Chen, C. Liu, J. Xu, J. Li and N. Yan, *Catal. Sci. Technol.*, 2012, **2**, 915-917.
14. L. Ma, J. Li, R. Ke and L. Fu, *J. Phys. Chem. C*, 2011, **115**, 7603-7612.
15. L. Ma, J. Li, Y. Cheng, C. K. Lambert and L. Fu, *Environ. Sci. Technol.*, 2012, **46**, 1747-1754.
16. C. Liu, S. Yang, L. Ma, Y. Peng, A. Hamidreza, H. Chang and J. Li, *Catal. Lett.*, 2013, **143**, 697-704.
17. C. Cristiani, M. Bellotto, P. Forzatti and F. Bregani, *J. Mater. Res.*, 1993, **8**, 2019-2025.
18. L. J. Alemany, L. Lietti, N. Ferlazzo, P. Forzatti, G. Busca, E. Giamello and F. Bregani, *J. Catal.*, 1995, **155**, 117-130.
19. J. W. Choung, I.-S. Nam and S.-W. Ham, *Catal. Today*, 2006, **111**, 242-247.
20. P. G. W. A. Kompio, A. Brückner, F. Hipler, G. Auer, E. Löffler and W. Grünert, *J. Catal.*, 2012, **286**, 237-247.
21. F. Liu, W. Shan, Z. Lian, L. Xie, W. Yang and H. He, *Catal. Sci. Technol.*, 2013, **3**, 2699-2707.
22. W. Shan, F. Liu, H. He, X. Shi and C. Zhang, *Chem. Commun.*, 2011, **47**, 8046-8048.
23. Z. Wu, R. Jin, H. Wang and Y. Liu, *Catal. Commun.*, 2009, **10**, 935-939.
24. F. Pérez-Robles, F. J. García-Rodríguez, S. Jiménez-Sandoval and J. González-Hernández, *J. Raman Spectrosc.*, 1999, **30**, 1099-1104.
25. I. E. Wachs and C. A. Roberts, *Chem. Soc. Rev.*, 2010, **39**, 5002-5017.
26. J. Engweiler, J. Harf and A. Baiker, *J. Catal.*, 1996, **159**, 259-269.
27. G. Giecko, T. Borowiecki, W. Gac and J. Kruk, *Catal. Today*, 2008, **137**, 403-409.
28. Z. Chen, F. Wang, H. Li, Q. Yang, L. Wang and X. Li, *Ind. Eng. Chem. Res.*, 2011, **51**, 202-212.
29. Z. Liu, Y. Yi, J. Li, S. I. Woo, B. Wang, X. Cao and Z. Li, *Chem. Commun.*, 2013, **49**, 7726-7728.
30. S. Roy, B. Viswanath, M. Hegde and G. Madras, *J. Phys. Chem. C*, 2008, **112**, 6002-6012.
31. S. Zhan, M. Qiu, S. Yang, D. Zhu, H. Yu and Y. Li, *J. Mater. Chem. A*, 2014, **2**, 20486-20493.
32. Y. Peng, K. Li and J. Li, *Appl. Catal. B- Environ*, 2013, **140–141**, 483-492.
33. Z. Wu, B. Jiang, Y. Liu, H. Wang and R. Jin, *Environ. Sci. Technol.*, 2007, **41**, 5812-5817.
34. A.-S. Mamede, E. Payen, P. Grange, G. Poncelet, A. Ion, M. Alifanti and V. Pârvulescu, *J. Catal.*, 2004, **223**, 1-12.
35. K. I. Hadjiivanov, *Catal. Rev.*, 2000, **42**, 71-144.
36. W. S. Kijlstra, D. S. Brands, E. K. Poels and A. Bliek, *Catal. Today*, 1999, **50**, 133-140.